DI-8 FATIGUE FRACTURE OF VACUUM-MELTED BALL BEARING STEEL

Takeo YOKOBORI* and Masatake NANBU**

ABSTRACT

Mechanical, metallographical and electron microfractographical studies were carried out in attempting to get fundamental knowledge concerning the initiation and propagation process of fatigue crack on the fatigue fracture surfaces of vacuum melted ball bearing quality steel of SUJ2.

In the case of the specimens, the axis of which is perpendicular to the direction of rolling, the fracture surface has the following four areas which can clearly distinguished as:

the area(a): the dark straight appearance, which has been identified as elongated inclusions of MnS type,
the area(b): a relatively smooth, white circular area with the area (a) in its centre,
the area(c): coarse area surrounding the area (b), and
the area(d): the fracture surface in the remaining part of the cross-section corresponding to the catastrophic static fracture.

On the other hand, in the case of the specimens, the axis of which is in the direction of rolling, fracture often originated at the tiny inclusions of MnS type open to the surface.

In the area (b) the tear dimples were very often observed, near the bottom of which cracked cementite particles were often observed. The area (c) is also considered as a kind of fatigue fracture surface.

1. INTRODUCTION

Whereas the studies with the microscope have now identified the stages of fatigue fracture fairly precisely in the case of pure materials or non-ferrous metals, there appears to exist not so many fundamental fatigue studies on commercial steels, especialy, on high hardened steels. The present study was carried out to investigate the initiation and propagation process of fatigue crack on the fatigue fracture surfaces of vacuum melted ball bearing quality steel of SUJ2.

2. MATERIAL AND EXPERIMENTAL PROCEDURE

The steel used was a vacuum melted ball bearing quality steel having spheroidized structure. The spheroidized structure was obtained by heat treatment. The analysis of the steel is given in Table I. The content of

* Professor of Mechanical Engineering, Tohoku University, Sendai, Japan
** Assistant, Tohoku University, Sendai, Japan

nonmetallic inclusion is shown in Table II. The authors would like to express their grateful thanks for the material preparation to Fujikoshi steel making Co. Ltd.

The longitudinal and transverse specimens were taken from the parent bar stock as shown in Fig.1. The location being subjected to the maximum applied stress among the perimeter of the specimen during each stress cycle of reversed bending was predetermined as illustrated in Fig.1. That is, the position of the cotter plane of the chucking part of the specimen in the parent bar stock was decided to be parallel to the tangential plane at the location of maximum stress of the specimen perimeter to the concentric cylinder with the parent bar stock, passing the location of maximum stress also. The specimens were machined into the shape and dimensions as illustrated in Fig.1.

After the machining, the specimens were held for 25 minutes at 835°C, and oil quenched (60-80°C), and then tempered for 4 hours at 160°C. The hardness obtained was Rockwell C-62. The heat treatment was carried out by ball bearing manufacturing Co., Nippon Seiko Kabushiki-kaisha (NSK), whom the authors would like to thank. The specimens were ground and the final surface finishing was carried out with 0000 emery papers.

The fatigue tests were conducted using Schenk fatigue testing machines operated at speeds of 2,850 rpm. under the reversed bending stresses.

Metallographic and electron microscopic studies were carried out.

3. EXPERIMENTAL RESULTS AND DISCUSSION

S-N relations are illustrated in Fig.2. Microscopic examination of the fracture surfaces was made with special reference to the inclusions. Results show that in the case of longitudinal specimens, the fractures often originated at small inclusions which were open to the specimen surface. Fig.4-1 shows a transverse cross section of the longitudinal specimens as appeared on the fracture surface.

On the other hand, the fracture in the case of transverse specimens initiated the crack at inclusions open to the surface, or were at various depths below the surface, depending upon the magnitude of the stress amplitude. At higher stress amplitude the fracture often originated at inclusions open to the surface, and at lower stress amplitude the fracture originated at inclusions slightly below the surface. That is, at 95 Kg/mm^2 of fatigue stress 80% of the specimens initiated the crack at the inclusion open to the surface, and at 85 Kg/mm^2 60% of them initiated the crack at the inclusion below the surface.

In the case of the fracture originated at inclusions slightly below the surface, that is, in the case of transverse specimens, the following four areas which can be cleary distinguished were observed in present studies:

the area(a): the dark straight appearance,

the area(b): a relatively smooth, white circular area with the area (a) in its centre,

the area(c): coarse area surrounding the area (b), and

the area(d): the fracture surface in the remaining part of the cross section corresponding to the catastrophic static fracture.

They are shown respectivelly in Figs.3 and 4. That is, the fracture surface may correspond to so-called "fish-eye",[1)2)3)4)***] although the definition of "fish-eye" is not identified.[5)] Of course, there is no reason for believing that all the similar fracture surfaces called "fish-eye" have the same mechanism.[5)] In fracture problems apparently similar phenomena are often caused by different mechanisms. On the other hand, it is of considerable importance to study the fatigue crack initiation and propagation process of vacuum melted ball bearing quality steel of SUJ2 in connection with the characteristic fish-eye pattern in the commercial SUJ2 ball bearing steel[1)] and the fundamentals of the fatigue crack intiation and propagation of high strength steels, since similar fish-eye are reported to be observed in such high hardened steels[6)] and an ausformed steel[7)] also. We might benefit from comparing similarities in approaches and results as well as from emphasizing the microstructural differences in various materials.

In present studies, the dark narrow area (a) in transverse specimens was identified as inclusions by the following metallographic examination on the fracture surface. Figs.4-2 and 4-3 show a transverse cross section of the transverse specimen as appeared on fracture surface. In the case of longitudinal specimens the dark narrow appearances were not observed as shown in Fig.4-1. Thus it is noted that there was appreciable elongation of the inclusion in the longitudinal direction, which shows it is malleable at the rolling temperatures of the steel. Micro-Vickers hardness test showed much lower hardness in the area (a) than in the area (b) and (c). An electronprobe microanalysis of the area (a) on the fracture surface showed high concentration of manganese and sulphur. This evidence suggested that the inclusion acting as crack origin was MnS type inclusions. In Fig.5 some of the results are shown.

In some case we found the following two characteristics. Firstly in the case of the transverse specimens the crack branches appeared to initiate mostly at the neighborhood of the tip of the inclusion as shown in Fig.4-3 and Fig.6-1. Secondary, the ratio[8)] of the bending fatigue strength of the transverse specimen to that of the longitudinal specimens is about 0.89 at the life of 1.5×10^6 although the inclusion initiating the fatigue crack in transverse specimens is the inclusion elongated to longitudinal direction of the parent bar in this case.

The area (b) was not visually clearly distinguished from the area (c) in the specimens the failures of which had originated at inclusions open

*** During carrying out the fatigue tests on the ball bearing steel as a part of the research project of 129 Committee (See ACKNOWLEDGEMENT), such pattern has been found on the fracture surface.[1)2)3)4)]

to the surface as shown in Figs.4-1 and 4-2.

A plot of inclusion size versus fatigue life at the same magnitude of stress amplitude showed no systematic correlation between the two variables, although Commings et al[9] showed the fatigue life decreases with increase of the size of the inclusion. This is why most of the fatigue crack initiated at elongated inclusion and at various depths below the specimen surface in the present set of specimens. Thus in such subsurface crack we attempted to plot the fatigue life against the stress σ_i calculated by the following formula: $\sigma_i = \sigma (R-d)/R$, where σ = the nominal applied peripheral stress, 2R = the specimen diameter and d = the depth of the centre of the inclusion from the tangential plane at the location of maximum stress of specimen perimeter. No systematic correlations, however, can be found between stress σ_i and fatigue life.

The electron microfractographical study was carried out. The plastic film was used to replicate fatigue fracture surface. The replicas were made by shadowing this plastic replica with chromium (at 45°) and then carbon (normal to the surface) in vacuum evaporator. Fig.6-1 shows the boundary between the area (a) and (b). The river pattern can be seen initiating from the extruded inclusion. In some cases, on each of the two halves of the fracture surface we found the characteristic tear dimples[10] in the area (b). These dimples having the shape of parabola point toward the fracture origin on each of the two halves of the fracture surfaces. That is, they point toward the inclusion initiating fracture. Figs.6-2 and 6-3 show typical examples of elongated tear dimples appeared on each of the two halves of the fracture surfaces. The arrows in Figs.6-2, 6-3, 6-4 and 6-5 indicate the direction of crack propagation. Cementite particles having river pattern were frequently observed near the bottom side of the tear dimples mentioned above as shown in Figs. 6-4 and 6-5. This appearance suggest that microcrack may have been initiated by cleavage fracture of the cementite particles or by decohesion between the matrix and the cementite particles. Such microcrack may correspond to the tear dimple in the present microfractograph on fatigue fracture part (b). In the case of static fibrous rupture of metals, the similar trend has been studied by Crussard et al.[11] These microcracks or voids, in turn, may be individually intersected by, and coalesce with, the tip of a growing fatigue crack, just as suggested by Beachem[10] in static ductile rupture in metals. By this inference it may be considered that the density and shape of cementites will affect patterns of tear dimples and thus the crack propagation of fatigue crack. Each tear dimples may not represent successive possitions of the crack fronts, because generally the voids growth and coalescence with the main crack might require a few cycles of stress at least since the strain is very small.

Fig.6-6 shows the boundary between the area (b) and (c), and Fig. 6-7 shows the area (c). Very often, in the area (c) the equiaxed dimples are observed. Further the pattern apparently like austenite grain boundary was frequently observed. The striation, however, which is inherent

to the fatigue of non-ferrous metals,[12] were difficult to be observed. In the area (c) the parallel pattern was sometimes observed being characteristic of fatigue fracture surface[13] as shown in Fig.6-8. Thus we cannot believe the fracture of the area (c) was caused statically, catastrophically by applied load as a result of the reduction of load-carrying area due to the opening of the crack (b). It also may be concluded if we consider the magnitude of the static tensile fracture strength of this steel as shown in Fig.7 and also the ratio of the size of the area (b) to the total cross sectional area of the specimen. That is, the fracture of the area (c) should be regarded as a kind of fatigue fracture.

On the other hand, obviously there must have been some possibility of the fracture surface having been compressed during compressive cycles. However, as far as this effect is concerned both the area (b) and (c) must have been affected almost equally. Therefore, we cannot help considering the different appearance between the area (b) and (c) is essential from the standpoint of the mechanism. One tentative explanation of the different appearance between (b) and (c) may be two conditions during crack propagation: During (b) the crack grew beneath the surface in the absence of air, whereas during (c) it grew with air present, although in ausformed steel Borik et al[7] considered (a) and (b) respectively corresponding to (b) and (c) in our study. It is of considerable interest that the characteristics are very similar between the ball bearing steel and an ausformed steel of almost the same hardness of HRC61-HRC62. In the case of an ausformed steel[7] the area (b) is far much larger, say extending to almost half the cross section radius, and the fatigue strength is much higher than the ball bearing steel as shown in Fig.8. Therefore, it appears that the steel with the large area (b) attained before the fatigue stage (c) occured may have the higher fatigue strength when with the same high hardness.

4. CONCLUSIONS

(1) Most of the fatigue fracture of vacuum melted ball bearing quality steel generally initiate at the inclusions.
(2) In the case of transverse specimens, the fracture surface has the following four areas which can be clearly distinguished:
the area(a): the dark straight appearance
the area(b): a relatively smooth, white circular fracture surface,
the area(c): coarse fracture surface, and
the area(d): the fracture surface in the remaining part of the cross-section corresponding to characteristic static fracture.
(3) The area (a) corresponds to the elongated MnS type of inclusions.
(4) The area (b) shows the electronmicroscopic pattern having tear dimple. A cementite particles are frequently observed near the bottom of the tear dimple. The density and shape of cementite particles may affect the pattern of the tear dimple and thus the crack propagation of fatigue crack.

(5) The area (c) shows the electron-microscopic pattern having equiaxed dimple. The parallel pattern being one of the characteristics of fatigue fracture was sometimes observed. The area (c) is a kind of fatigue fracture surface.

(6) Comparing with the similar characteristics appeared on the fatigue fracture surface of an ausformed steel, super high strength steel with the same hardness, it may be that the steel with the larger area (b) has the higher fatigue strength, when with the same high hardness. The need is emphasized to determine the factors which control the change from the (b) process into the (c) process.

ACKNOWLEDGEMENT

The study was a part of the research project of the Sub-Committee on "The Relation of the Inclusions and the Structures to Mechanical Behavior" of 129 Committee (The Strength, Fracture and Fatigue Committee) of the Japan Society for Promotion of Science. The authors' thanks are due to the committee members for their co-operation throughout the investigation. Especially the authors wish to thank Prof. T. Ichinokawa, Waseda University for electronprobe microanalysis on the inclusions, and Dr. M. Kondo, Director, Central Res. Lab. Fujikoshi Steel Co. for material preparation, and Dr. T. Hatori, Technical Director, Nippon Seiko ball bearing Co., for heat treatment.

REFERENCES

1) T. Yokobori and M. Nanbu, Fish Eye Appearing on the Fatigue Fracture Surface of Ball Bearing Steel, Proceedings of the 2nd Conference on Dimensioning and Strength Calculations, Hungrian Academy of Sciences, Budapest, 1965, P.459
2) H. Muro, The Internal Report of 129 Committee, No.1-14-3 (1963) (In Japanese)
3) Y. Kawada, H. Nakazawa and S. Kodama, "The Effects of the Shapes and the Distributions of Inclusions on the Fatigue Strength of Bearing Steels in Rotary Bending", Trans. Japan Soc. Mech. Engrs. Vol.29 (1963) P.1674 (In Japanese)
4) Daido Steel Co. Group, The Internal Report of 129 Committee No.1-15-3 (1963) (In Japanese)
5) R. E. Peterson, Handbook of Experimental Stress Analysis, M. Hetenyi Ed., New York, John Wiley and Sons (1950) P.615.
6) H. E. Frankel, J. A. Bennett, and C. M. Carman, "Fatigue Properties of Some High-Strength Steels, Proc. Am. Soc. Testing Materials, Vol. 60 (1960) P.501.
7) F. Borik, W. M. Justusson and V. F. Zackay, "Fatigue Properties of an Ausformed Steel." Trans. ASM, Vol.56 (1963) P.327.
8) T. Yokobori and I. Maekawa, "An Anisotropy of Fatigue Strength of Ball Bearing Steels," The Report of 129 Committee, No.1-2 (1961) (In Japanese)

9) H. N. Cummings, F. B. Stulen, and W. C. Schulte, "Relation of Inclusions to the Fatigue Properties of SAE 4340 Steel," Trans. ASM, Vol.49 (1957) P.482.
10) C. D. Beachem. "An Electron Fractographic Study of the Influence of Plastic Strain Conditions Upon Ductile Rupture Processes in Metals." Trans. ASM, Vol.56 (1963) P.318.
11) C. Crussard et al, Fracture, B. L. Averbach et al Ed., MIT, 1959, P.524.
12) P. J. E. Forsyth, "A Two Stage Process of Fatigue Crack Growth," Crack Propagation Symposium, Cranfield, College of Aeronautics (1962) P.76.
13) Akira Tokuda, "Observation of the Fatigue Fracture Surface of Some Carbon Steels by Electron Microscope". Trans. JIM, Vol.1 (1960) P.108: Vol.2 (1961) P.239.

Table I. Chemical composition, per cent by weight

Specimen symbol	C	Si	Mn	P	S	Cu	Ni	Cr
84V	1.02	0.25	0.31	0.017	0.008	0.11	0.07	1.44

Table II. Inclusion Rating

Specimen symbol	dA (A-type)	dB (B-type)	dC (C-type)	d (Total)
84V	0.013	0.004	0.004	0.021

A-type corresponds to inclusions deformed malleably by working and often elongated.
B-type corresponds to inclusions of particle type alined discontinuously in group in the direction of working.
C-type corresponds to not malleable inclusions of particle type dispersed irregularly.

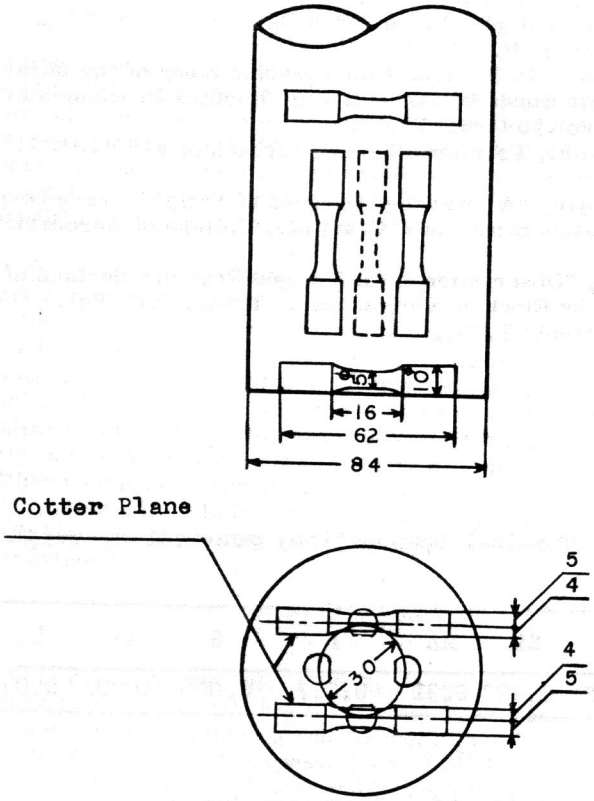

Fig.1 Sectioning of material into fatigue specimens and dimension of them.

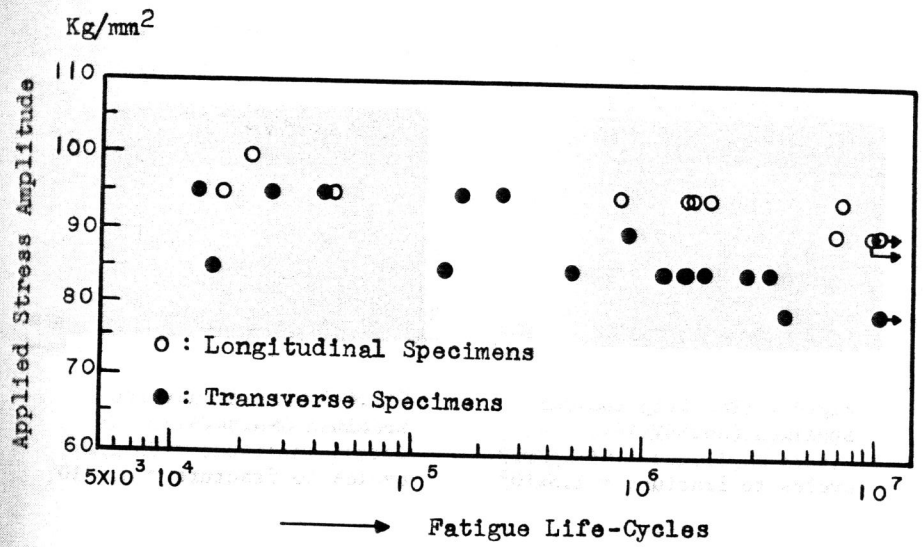

Fig.2 S-N plots of fatigue specimens.

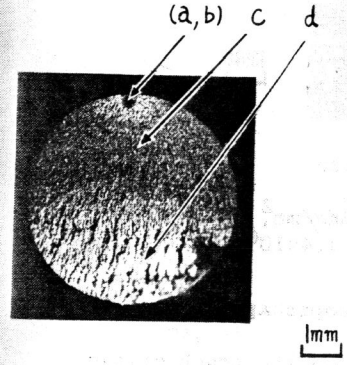

Fig.3 A typical example of the overall visual appearance of the fatigue fracture surface.
Specimen No.84VB8, stress amplitude = 85Kg/mm^2, cycles to fracture = 1.78×10^6.
a,b and c are the same notions as in Fig.4.
d = the remaining part of the cross section corresponding to the catastrophic static fracture.

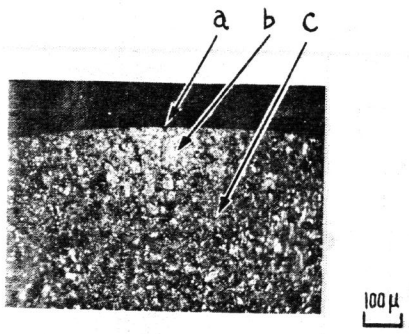

Fig.4-1 The longitudinal specimen (No.84VA16).
stress amplitude = 95 Kg/mm^2,
cycles to fracture = 1.5×10^6.

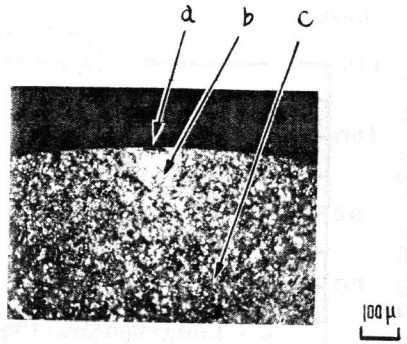

Fig.4-2 The transverse specimen (No.84VB11).
stress amplitude = $95 Kg/mm^2$,
cycles to fracture = 2.5×10^4.

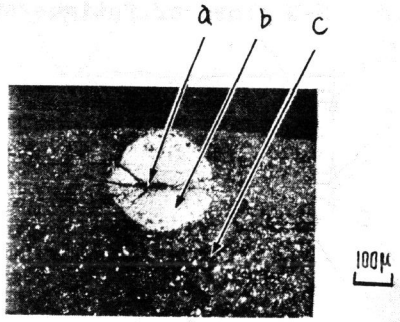

Fig.4-3 The transverse specimen (No.84VB3).
stress amplitude = $85 Kg/mm^2$,
cycles to fracture = 1.4×10^6.

Fig.4 Typical examples of the microscopic appearance of the fatigue fracture surfaces.
a = the non-metallic inclusion as the crack origin
b = relatively smooth area coresponding to the apparent critical crack
c = coarse area

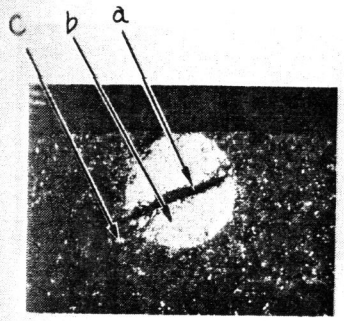

Fig.5-1 Optical image of the site analysed.

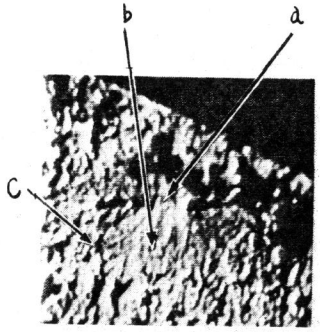

Fig.5-2 Electron image. The same site as shown in Fig.5-1.

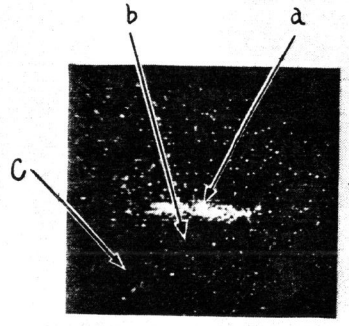

Fig.5-3 X-ray image by MnK_α. The same site as shown in Fig.5-1.

Fig.5 Typical example of the results by electronprobe micro-analysis. From Figs. 5-1 to 5-3 : Specimen No. 84VB5, stress amplitude = $85 Kg/mm^2$, cycles to fracture = 1.41×10^6.

Fig.6 Typical examples of the electron microfractographs on the fatigue fracture surfaces.

Fig.6-1 Shows the boundary between the inclusion (a) and the area (b).
Specimen No.84VB5,
stress amplitude = 85Kg/mm^2,
cycles to fracture = 1.41×10^6.

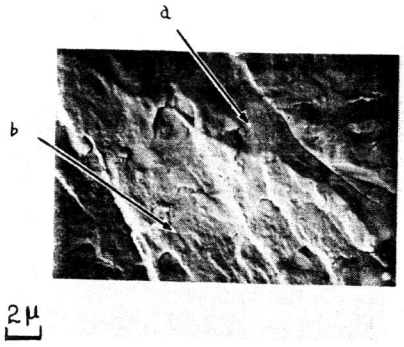

Fig.6-1

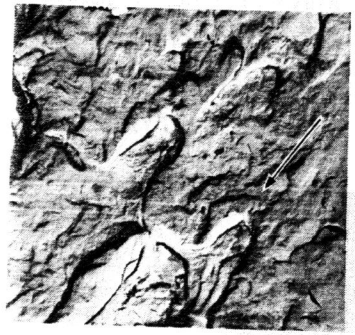

Fig.6-2 1μ

Fig.6-3 1μ

Figs.6-2,6-3. Show the tear dimples in the area (b) appeared on the two halves of fracture surfaces of the same specimen.
Specimen No.84VB3, stress amplitude = 85Kg/mm^2, cycles to fracture = 1.4×10^6.

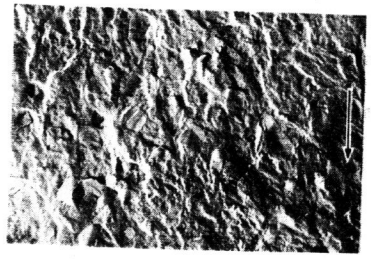

Fig.6-4 Shows the cementite particles in the area (b). The same surface as shown in Fig.6-1.

3μ

Fig.6-4

1μ

Fig.6-5 Shows the tear dimples in the area (b).
The same specimen as shown in Figs.6-2 and 6-3.

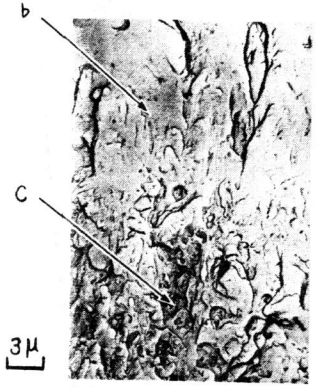

Fig.6-6 Shows the boundary between the area (b) and the area (c).
The same specimen as shown in Figs.6-2 and 6-3.

2μ

Fig.6-7 Shows the area (c).
Specimen No.84VA11,
stress amplitude = 95Kg/mm^2,
cycles to fracture = 6.9×10^6.

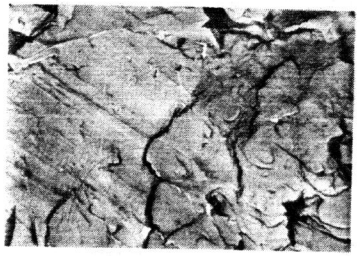

1μ

Fig.6-8 Shows the parallel pattern in the area (c).
The same specimen as shown in Figs. 6-2 and 6-3.
This pattern was taken from the area (c) near the boundary of the area (b) and (c).

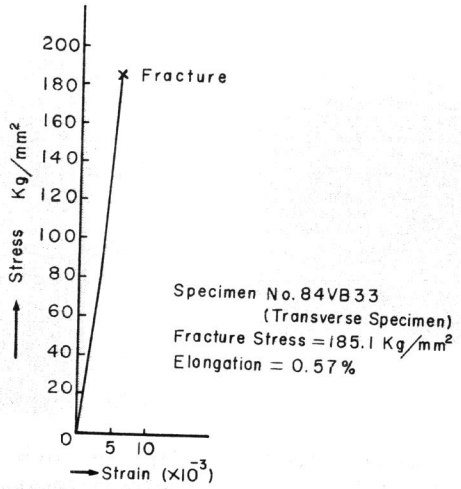

Fig. 7 Typical tensile stress strain curve of vacuum melted ball bearing quality steel.

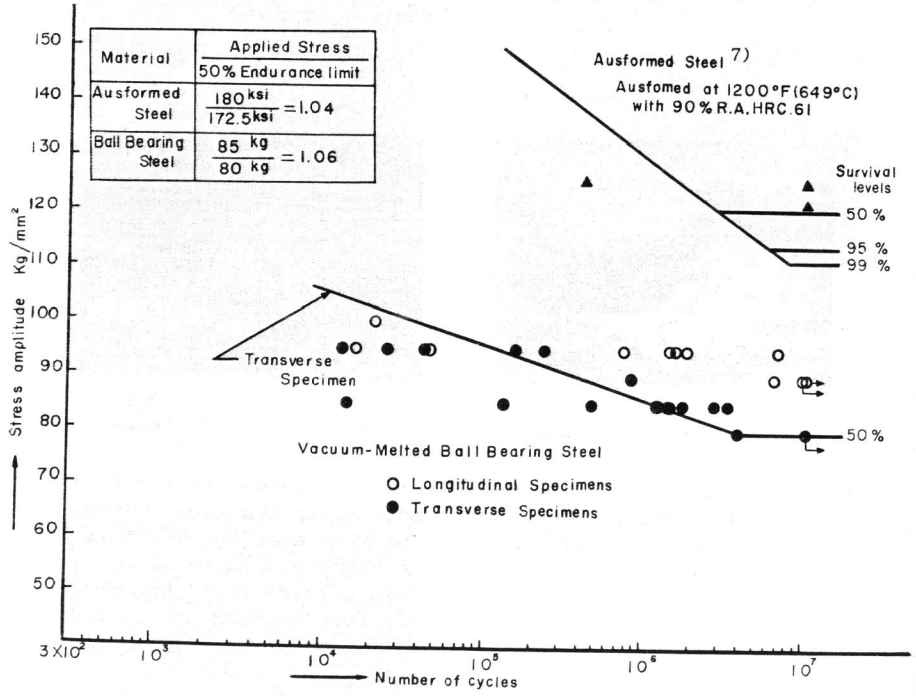

Fig.8. S-N curves of the vacuum-melted ball bearing steel and ausformed steel. The comparison of the fatigue life has been made at the equivalent stress level, that is, approximately the same value, 1.04 to 1.06, of the ratio of the applied stress amplitude to the endurance limit.